

Measurement of resistance and spin-memory loss (spin relaxation) at interfaces using sputtered current perpendicular-to-plane exchange-biased spin valves

Wanjun Park, David V. Baxter,* S. Steenwyk,† I. Moraru, W. P. Pratt, Jr., and J. Bass

Department of Physics, Center for Fundamental Materials Research, and Center for Sensor Materials, Michigan State University, East Lansing, Michigan 48824-1116

(Received 10 January 2000)

We describe measurements using a technique for determining interfacial resistances and loss of spin-direction memory (spin relaxation) for nonmagnetic metals and nonmagnetic interfaces. The technique involves inserting the metal of interest, or a multilayer, into the middle of a current-perpendicular (CPP) permalloy-based exchange-biased spin-valve and monitoring the resulting increase in CPP resistance and decrease in magnetoresistance. The technique has the advantage over earlier ones of giving both uniform current and control of the required magnetic states. We test and validate the technique using (a) an alloy, CuPt (6 at. %), in which the spin-diffusion length has previously been measured with a different technique, (b) a metal, Ag, where we expect a long spin-diffusion length, and (c) Cu/Ag interfaces, where we expect little if any spin-memory loss. We then use the technique to measure spin-memory-loss (the spin-diffusion length) at 4.2 K of the antiferromagnetic alloy FeMn, which is used for pinning the ferromagnetic layers in our spin-valves, and of sputtered single layers of V, Nb, and W preparatory to measuring interfacial resistance and interfacial spin-memory loss in sputtered $[\text{Cu}/\text{Ag}]_N$, $[\text{Cu}/\text{V}]_N$, $[\text{Cu}/\text{Nb}]_N$, and $[\text{Cu}/\text{W}]_N$ multilayers with N repeats. To our surprise, we discovered large interfacial spin-relaxation rates for V/Cu, Nb/Cu, and W/Cu interfaces. These rates seem to be understandable as due to spin-orbit coupling in high resistivity interfacial alloys.

I. INTRODUCTION

Spin-polarized transport in ferromagnetic (F) metals, where the scattering of conduction electrons depends upon the relative directions of the electron spin and the local magnetization \mathbf{M} , has been studied since the 1970s.¹ Interest in the topic exploded recently after the discovery of giant magnetoresistance (GMR) in ferromagnetic-nonmagnetic (F/N) metal multilayers,² and rapid progress to GMR-based technology.³ It was recognized early on that spin-relaxation (loss of spin-direction-memory) could degrade spin-polarization.¹ Initial studies were limited to spin-current mixing due to scattering by phonons or magnons, which requires temperatures high enough to produce significant phonon and magnon populations.^{1,4} Recent studies of spin-current mixing are reviewed in Ref. 5.

Only more recently was it recognized^{4,6,7} that spin-relaxation could be important even at low temperatures (e.g., 4.2 K) where scattering by phonons and magnons is negligible, and that such relaxation might remain dominant to high temperatures. Low temperature spin-relaxation is attracting increasing attention,⁵⁻¹⁶ but is still inadequately understood. In this paper we describe in detail, test, and implement a new low-temperature detector in the current-perpendicular to the plane (CPP) geometry¹⁷ that allows fairly straightforward measurements of the resistances of N_1/N_2 interfaces and of spin-relaxation within N metals or alloys and at N_1/N_2 interfaces. The technique was first applied in Ref. 16.

Spin-relaxation within N metals was first studied by Johnson and Silsbee⁶ and Johnson.⁹ We and others later extended measurements to N alloys^{10,13} and to F metals and

alloys.^{7,12} The techniques of the previous studies of N layers did not give complete control over the two magnetic states needed for a rigorous analysis, the ones in which the magnetizations \mathbf{M} of adjacent F layers are aligned parallel (P) or antiparallel (AP) to each other. We achieve such control by means of a permalloy (Py)-based exchange-biased spin-valve (EBSV) geometry¹⁸, where a layer of the antiferromagnetic (AF) metal FeMn adjacent to one Py layer (the ‘‘pinned’’ layer) constrains that layer’s \mathbf{M} so that it reorients only at a much higher field than that needed to reorient the \mathbf{M} of a second, identical-thickness Py layer (the ‘‘free’’ layer). The two Py layers are separated from each other by an N layer thick enough to eliminate any exchange coupling between them. The only measurements of spin-relaxation at interfaces known to us are those from ESR studies of interfaces of alkali metals with Cu, Mn, and Al (Ref. 19) and the preliminary report¹⁶ of our Cu/Nb multilayer data. The ESR studies led to the belief⁴ that any spin-relaxation at interfaces is small. In contrast, we show that spin relaxation at some interfaces can be substantial.

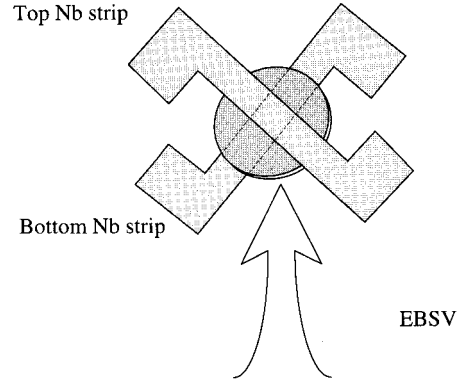
Since there should be few paramagnetic impurities in our Cu or the inserts, the spin-relaxation we study should be dominated by spin-orbit coupling. To allow a simple study of spin-orbit coupling, we chose Ag, which is chemically similar to Cu and where we expect to find a long spin-diffusion length, and the three metals V, Nb, and W, which are chemically similar to each other.²⁰ Since spin-orbit coupling increases with increasing row in the periodic table,²¹ we expect spin-relaxation to increase from V to Nb to W. Ag, V, Nb, and W are all nearly insoluble in Cu,²² so interface intermixing should occur only during deposition. The Nb and V layers are thin enough so that, sandwiched between Cu and ferromagnetic Py layers, they remain non-superconducting at

our measuring temperature of 4.2 K; in fact, our thickest Nb layer, $t_{\text{Nb}}=20$ nm, remained normal down to about 2.7 K. We test and validate our detector in three ways. First, quantitatively using an alloy of CuPt (6 at.%)—hereafter just CuPt—where the spin-relaxation length, the spin-diffusion length $l_{\text{sf}}^{\text{CuPt}}$, is dominated by spin-orbit coupling associated with the heavy Pt impurity and was previously measured with a different technique.¹⁰ Second, qualitatively with sputtered Ag, where we expect $l_{\text{sf}}^{\text{Ag}}$ to be long. Third, also qualitatively, with [Cu/Ag] interfaces, which should give little or no spin-memory loss. We then study spin-memory loss in single layers of antiferromagnetic FeMn, because of its role in our EBSVs, and in V, Nb, and W, mainly because we need their parameters for our studies of [V/Cu], [Nb/Cu], and [W/Cu] interfaces, but also to get a feeling for the sizes of l_{sf} in sputtered multilayers of these metals. We note that values of l_{sf} at 4.2 K for nominally “pure” metals are not quantitatively transferrable, because they are determined by the particular residual defects (impurities and point, line, and surface—e.g., stacking faults) produced by a given preparation system. The simple exponential decay of our data with increasing layer thickness at least shows that the defects in our samples do not vary substantially with layer thickness. Lastly, observation of systematic variations in interface resistance, and systematically different spin-memory loss, for interfaces of Cu with Ag and the three chemically similar metals V, Nb, and W, lets us rule out spurious results due to accidental magnetic contamination of any single type of interface.

II. SAMPLES AND PRINCIPLES OF THE TECHNIQUE

Our sample preparation, characterization, and sputtering techniques, and our method of measuring the CPP-MR have been described elsewhere.²³ The basis of the present technique is our standard method of crossed ~ 1 mm wide, 250 nm thick superconducting Nb strips,²³ used to produce uniform current flow through the area $A \sim 1.1$ mm² of the sample of interest—here our EBSV-based spin-relaxation detector. In the present study we sputtered a 10 nm thick Cu layer on top of the bottom Nb strip to help the AF-metal FeMn grow in the proper crystal structure for pinning²⁴ and a 10 nm Cu layer just below the last Nb strip to minimize the saturation field H_s of the topmost Py layer. Separate studies have shown that these Cu layers become superconducting by the proximity effect, so that the S/FeMn and S/Py interface specific resistances between each superconductor and its neighboring F-layer or AF-layer remain the same for the Nb/Cu bilayers as for a bare Nb layers. The crossed-strip geometry lets us directly measure the experimental quantities of interest²⁵ for our detector: its specific resistances (area A times resistance R) for the two magnetic states $AR(AP)$, $AR(P)$, and the difference between them, $A\Delta R = AR(AP) - AR(P)$.

The detector, sandwiched between the Nb strips, consists of a sputtered Py-based CPP-EBSV, in the middle of which is placed the insert X of interest as shown in Fig. 1. The EBSV consists of two equal thickness ($t_{\text{Py}}=24$ nm) layers of Py separated by a Cu layer thick enough ($t_{\text{Cu}}=20$ nm) to magnetically decouple the Py layers. We chose $t_{\text{Py}} \gg l_{\text{sf}}^{\text{Py}} = 5.5$ nm to make the signal of interest insensitive to small



Cu(10nm) capping layer
Py(24nm)
Cu(10nm)
X layer
Cu(10nm)
Py(24nm)
FeMn(8nm)
Cu(10nm)

FIG. 1. Sample structure showing the Nb cross strips and the EBSV with insert X .

sample-to-sample fluctuations in t_{Py} (Ref. 7) and because large t_{Py} simplifies the analysis as described in Sec. III. Detailed studies of $AR(AP)$, $AR(P)$, and $A\Delta R$ for Py-based EBSVs without inserts have already been published.⁷ Fig. 2 shows that both the magnetization M and AR for a control EBSV (with no inserted X layer) show the required sharp transitions between P and AP states and constant values in

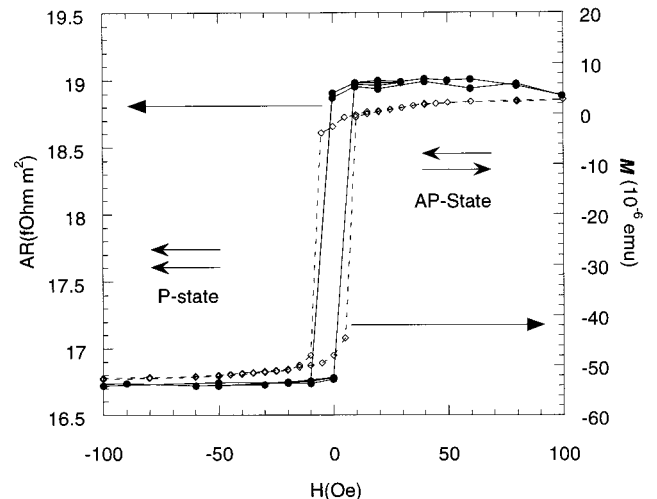


FIG. 2. AR (filled circles) and magnetization (M) (open diamonds) hysteresis curves for a Py-based EBSV without an insert.

each state. The insert X within the Cu layer can be either a single N layer of thickness t_N , or a multilayer with N bilayers—the number of bilayers N is italicized to distinguish it from N for the nonmagnetic metal. The effect of such an insert on the spin-valve signal is demonstrated in Fig. 3, which compares the $A\Delta R$ hysteresis loops for a control spin valve with those from spin valves with inserts of $X = \text{Ag}$, CuPt, V, Nb, and W. The basic principle of the detector is that spin relaxation in X will cause $A\Delta R$ to decrease exponentially with t_N or N , and measurement of that decrease will allow extraction of the magnitude of the spin relaxation. In practice the situation is slightly more complicated since the inserted layer or multilayer increases the resistance of the structure in addition to providing avenues for spin relaxation.

Both spin relaxation and the added resistance introduced by the insert can reduce the $A\Delta R$ of our EBSV structures. If the relaxation rate is not too large, and is dominated by processes in the bulk of the inserted layer, then the Valet-Fert (VF) theory⁴ predicts that

$$A\Delta R \propto \exp[-t_X/l_{sf}^X]/(AR_0 + AR_x). \quad (1)$$

The proportionality constant depends on the bulk and interface spin anisotropy parameters for Py, t_X and l_{sf}^X are the thickness and spin diffusion lengths of the insert, AR_0 is for the contribution to the denominator from the EBSV without the insert, and AR_x is the specific resistance increase associated with the insert. If spin relaxation is dominated by interfacial processes we may modify the above result to the form

$$A\Delta R \propto \exp\{-2N\delta\}/(AR_0 + AR_x), \quad (2)$$

where $2N$ is the number of inserted interfaces and $\delta = t_I/l_{sf}^I$ is the ratio of the interface thickness to its spin diffusion length. AR_0 and AR_x have the same meaning as in Eq. (1) and we note that the latter has both interface and bulk contributions $AR_x = N(\rho_N t_N + \rho_{Cu} t_{Cu} + 2AR_{Cu/N})$. In most cases the $\rho_{Cu} t_{Cu}$ term is negligible.

Even with no spin-relaxation in X (i.e., $l_{sf}^N = l_{sf}^{Cu/N} = \infty$), the term AR_x in the denominators of Eqs. (1) and (2) causes $A\Delta R$ to decrease algebraically with increasing t_N or N , in a way calculable from independent measurements of the properties of the component layers in the EBSV.

Spin-relaxation, in contrast, causes $A\Delta R$ to decrease exponentially as suggested by the numerators of Eqs. (1) and (2). The more rigorous equations actually used in our analysis are described in Sec. III. They account for spin relaxation both at the Cu/N interfaces and within the N layers, but assume that l_{sf}^{Cu} is so large that there is no spin-relaxation within the Cu layers. In this full theory the simple exponentials of Eqs. (1) and (2) are replaced by hyperbolic functions, but we shall see that the essential physics is well described by the above simplified forms.

III. EQUATIONS

Formally, our data are fit by solutions to equations derived for our multilayered samples using the two spin-channel (VF) theory for finite l_{sf} .⁴ For CPP current flow in a F/N multilayer, the VF theory describes the spin-polarized transport in terms of a splitting of the electrochemical potentials for the spin-up and spin-down electrons. Relations are

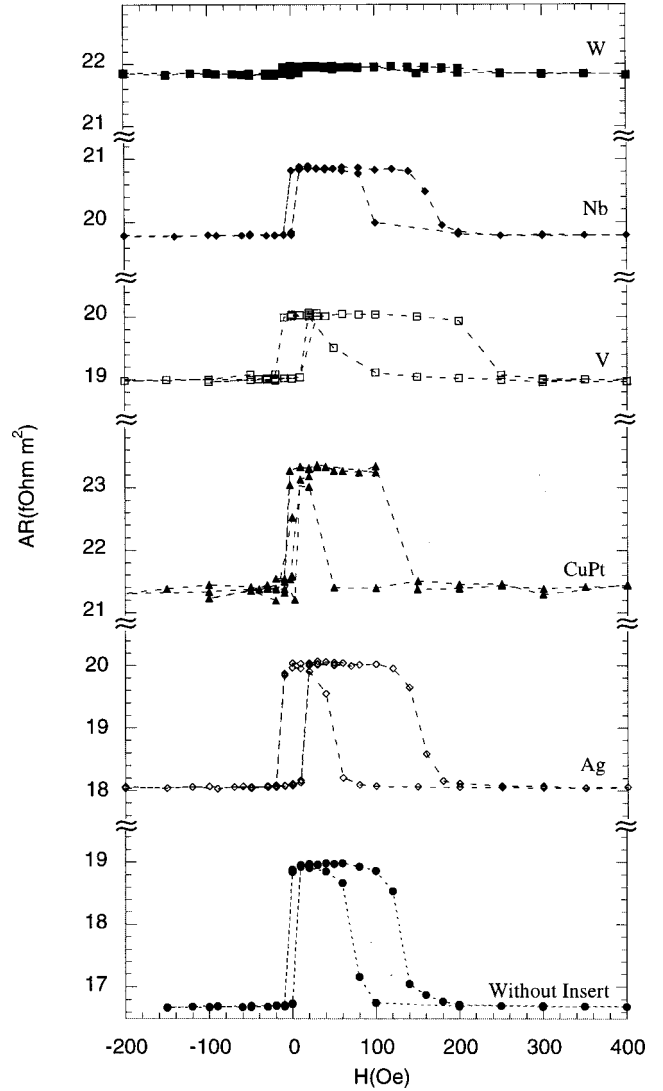


FIG. 3. AR hysteresis curves for Py-based EBSVs with no insert and with single layer, 3 nm thick inserts of Ag, CuPt(6 at. %), V, Nb, and W.

written for the spin-dependent, and spatially varying, chemical potentials and spin-dependent currents in each of the layers in the sample, and these relations are matched at the interfaces, taking account of interfacial specific resistances when needed but neglecting any interface-induced spin relaxation. In this theory, having $t_{Py} \gg l_{sf}^{Py}$ simplifies the computation of $A\Delta R$, because any nonequilibrium spin distribution in the Py layer resulting from the spin-polarized current flowing through the EBSV decays with distance from the Cu/Py interface over a length scale l_{sf}^{Py} . Thus the regions of the structure outside this distance from the Cu/Py interface (viz. the remainder of the Py layer, the FeMn layer, and the Py/S interfaces) make no contribution to $A\Delta R$; they only increase the total specific resistance of the structure AR .

Figure 4(a) shows the structural model used in adapting the VF theory to the case of a single N-layer insert (X), of nominal total thickness t_X , in the middle of the Cu layer. The Cu/N interface (I) is modeled as a uniform slab of resistivity ρ_I , spin-relaxation length l_{sf}^I and thickness t_I to which the Cu and N make equal contributions and for which δ

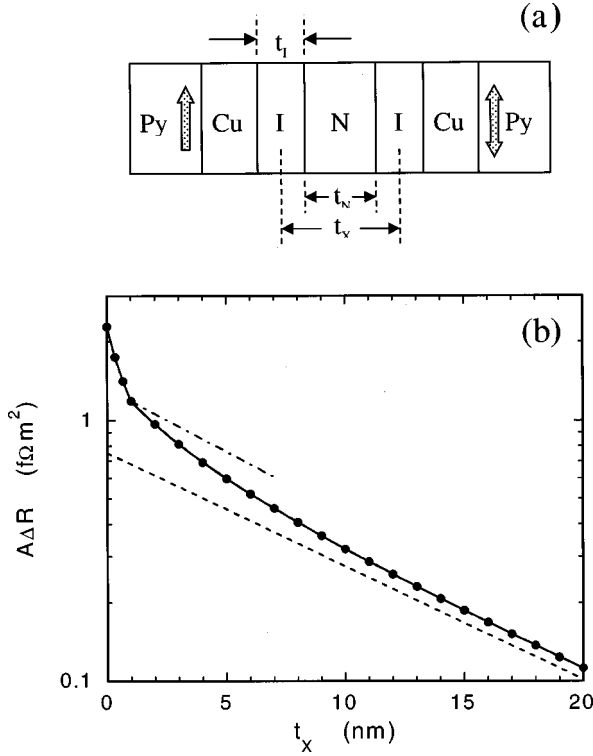


FIG. 4. (a) Simplified picture of an EBSV with a single N-layer insert (X) of total thickness t_X in the middle of the Cu layer. Each Cu/N interface slab has thickness t_I for $t_X \geq t_I$. (b) $A\Delta R$ vs t_X for solutions to Valet-Fert (VF) theory. Solid curve: numerical solution; solid circles: algebraic solution; dot-dashed curve: Eq. (1) (this curve overlaps with the solid curve for t_X below the “knee”); dashed line (vertical position arbitrarily set)=numerator of Eq. (1): $\exp(-t_N/l_{sf}^N)$ where t_N is the thickness of the bulk part of the N layer. The parameters for the VF solutions are $t_{Cu}=10$ nm, $t_I=1$ nm, $AR_{Cu/N}=2$ f Ωm^2 , $\delta=t_I/l_{sf}^I=0$, $\rho_N=100$ n Ωm , $l_{sf}^N=10$ nm, and $\beta_{Py}=0.76 \pm 0.07$ (see text). Other parameters are as in Ref. 7.

$=t_I/l_{sf}^I$. For $t_X \geq t_I$, one has $t_N=t_X-t_I$, where t_N is the thickness of the bulk part of the N layer and $AR_{Cu/N}=\rho_{Cu}t_{Cu}$. The bulk N layer is assumed to have spin-diffusion length l_{sf}^N , and the Cu layer, of thickness t_{Cu} and resistivity ρ_{Cu} , to have infinite l_{sf}^{Cu} . For $t_X < t_I$, the two overlapping interfacial slabs are treated as one slab with total thickness $=2t_X$, $t_N=0$, and ρ_I and δ the same as before.

The sample structure shown in Fig. 4(a) was chosen to be symmetric, which simplifies the VF equations because the spin-split chemical potentials have even and odd symmetry about the center of the N layer for AP and P states of the Py layers, respectively. Algebraic equations for $A\Delta R$ can then be obtained, as displayed below:

$$A\Delta R = 2(\beta\rho_{Py}^*l_{sf}^{Py} + \gamma AR_{Py/Cu}^*)^2 \left(\frac{1}{D_P} - \frac{1}{D_{AP}} \right), \quad (3)$$

where

$$D_{AP,P} = \rho_{Py}^*l_{sf}^{Py} + AR_{Py/Cu}^* + \rho_{Cu}t_{Cu} + \left(\frac{AR_{Cu/N}}{\delta} \right) \times \left(\frac{\frac{AR_{Cu/N}}{\delta} + (\rho_N l_{sf}^N) \coth(\delta) f_N^{AP,P}}{(AR_{Cu/N}/\delta) \coth(\delta) + (\rho_N l_{sf}^N) f_N^{AP,P}} \right) \quad (4)$$

with $f_N^{AP} = \coth(t_N/2l_{sf}^N)$ and $f_N^P = \tanh(t_N/2l_{sf}^N)$. For the Py layers, $\rho_{Py}^{\uparrow,(1)}$ is the resistivity and $AR_{Py/Cu}^{\uparrow,(1)}$ is the Py/Cu interface resistance for conduction electron moment parallel (antiparallel) to the magnetization, giving $\rho_{Py}^* = (\rho_{Py}^{\uparrow} + \rho_{Py}^{\downarrow})/4$ and $AR_{Py/Cu}^* = (AR_{Py/Cu}^{\uparrow} + AR_{Py/Cu}^{\downarrow})/4$. The anisotropy parameters β and γ are defined by $\beta = [(\rho_{Py}^{\downarrow} - \rho_{Py}^{\uparrow})/(\rho_{Py}^{\downarrow} + \rho_{Py}^{\uparrow})]$ and $\gamma = [(AR_{Py/Cu}^{\downarrow} - AR_{Py/Cu}^{\uparrow})/(AR_{Py/Cu}^{\downarrow} + AR_{Py/Cu}^{\uparrow})]$.

The parameters within the Py and at the Py/Cu interfaces are taken to be those published in Ref. 7, except that we have increased β from 0.73 ± 0.07 to 0.76 ± 0.07 to account for slightly larger values of $A\Delta R$ seen in our more recently produced Py-based EBSVs without inserts.²⁶

Fig. 4(b) shows $A\Delta R$ vs t_X for the VF theory as applied to the multilayer structure of Fig. 4(a), using parameters indicated in the figure caption. To obtain solutions to more complicated, less symmetrical multilayers, we usually solve the coupled linear-equation problem numerically; this numerical solution is shown as a solid curve. To simplify the solution for this plot, we have assumed that there is no spin relaxation in the Cu/N interfacial region ($t_I \ll l_{sf}^I$). The solid circles are the algebraic solution [Eqs. (3) and (4)]. As expected, the solid curve and the circles are indistinguishable. The dot-dashed curve represents Eq. (1), suitably normalized to agree with the exact solution at $t_X=0$. Equation (1) clearly provides a reasonable approximation to the expected behavior, especially for small t_X . The “knee” in the solid curve at $t_X=1$ nm ($=t_I$) occurs at the value of t_X where the two Cu/N interfaces become fully formed. Thus measurements of $A\Delta R$ for an EBSV can detect the formation of just two interfaces in the Cu layer between the two Py layers, so long as $AR_{Cu/N}$ is sufficiently large—see Eq. (1) discussion. The dashed curve indicates the exponential form, $\exp(-t_N/l_{sf}^N)$, from the numerator of Eq. (1). The slopes of the solid and dashed curves agree well at large t_X .

Figure 5(a) shows the assumed sample structure for a multilayer insert containing N [Cu/N] bilayers. The VF theory is first used to relate the two parameters of the spin-split chemical potentials in the Cu layers at each end of one unit cell via a simple 2×2 transfer matrix. Then the whole structure is solved numerically, including contributions from both Py layers. Figure 5(b) is a plot of $A\Delta R$ vs N . The solid curve is the solution for the parameters listed in the figure caption. The dashed curve indicates the exponential form of the numerator of Eq. (2). As expected, at large N the slopes of these curves are very similar.

IV. DATA AND ANALYSIS

We start with the data for single layer inserts. Figure 3 showed the AR hysteresis curves for EBSVs with 3 nm thick inserts of Ag, V, Nb, W, and CuPt. Similar curves are also

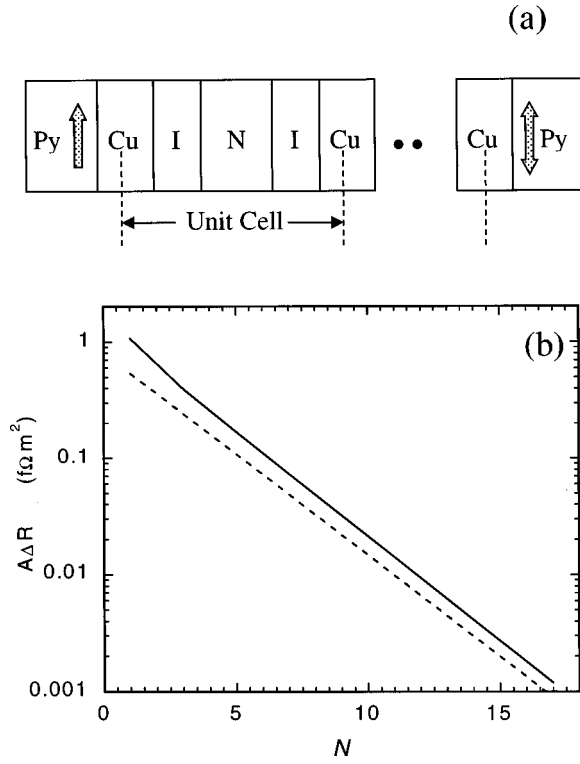


FIG. 5. (a) Sample structure for inserts containing N unit cells of [Cu/N] with Cu/N interfaces (I) as defined in Fig. 4 and the text. (b) $A\Delta R$ vs N for solutions to VF theory. Solid curve: numerical solution; dashed line (vertical position arbitrarily set): numerator of Eq. (1): $\exp(-2N\delta)$. The parameters are the same as for Fig. 4(b), except here $t_N = 1$ nm, $l_{sf}^N = \infty$, and $\delta = t_I/l_{sf}^I = 0.2$.

obtained for FeMn. As in Fig. 2, all of the data show sharp transitions between AP and P states and well defined constant values of AR in both the P and AP states. In contrast to Fig. 2, Fig. 3 shows data to fields in the positive direction sufficiently large to unpin the exchanged-biased Py layer.

Figure 6 shows the decreases in $A\Delta R$ with t_X for the samples of Fig. 4 plus FeMn (i.e., samples with a single layer inserted into the EBSV). CuPt was measured to test the new technique by determining a value of l_{sf}^{CuPt} to compare with the value $l_{sf}^{CuPt} = 8 \pm 2$ nm measured earlier with a completely different technique.¹⁰ The best fit (dotted curve in Fig. 6) gives a value of $l_{sf}^{CuPt} = 11 \pm 3$ nm that overlaps with the previous one. We take this overlap to validate both techniques to within their mutual uncertainties.

As a demonstration of our technique in a more general context we have also measured spin relaxation in the antiferromagnetic alloy FeMn used for the exchange-bias-pinning in our EBSV. The FeMn data in Fig. 6 fall off very rapidly with t_{FeMn} . The dashed curve is a fit with very strong interfacial spin relaxation $\delta = 2.5$ followed by a short $l_{sf}^{FeMn} \sim 1.5$ nm. Within uncertainties, the data can also be fit by a single line corresponding to slightly smaller value for δ .

Turning now to the four nominally “pure” metals, we see in Fig. 6 that $A\Delta R$ for $N = V, Nb,$ and W first decreases rapidly with increasing t_N and then more slowly. We ascribe the initial rapid decrease mostly to formation of the two Cu/N interfaces, which contribute to the denominator of Eq. (1) [and to the numerator if δ is large enough for Eq. (2) to be more appropriate]. This ability to see the two interfaces

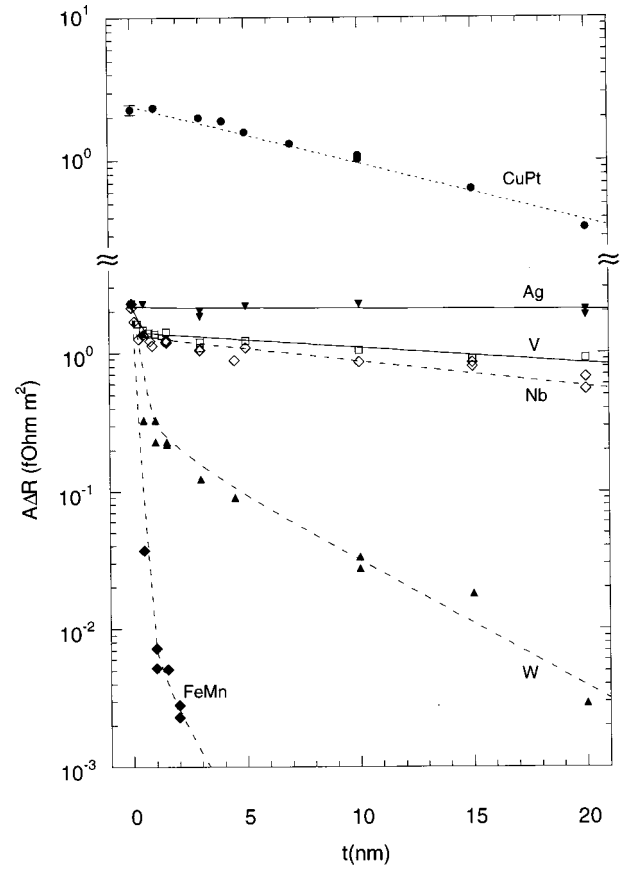


FIG. 6. $A\Delta R$ vs t_N for single layer inserts of CuPt, FeMn, Ag, V, Nb, and W. The solid curves are fits assuming $l_{sf}^N = \infty$. The dotted and dashed curves are fits with the values of l_{sf}^N given in Table I.

form is important, as it lets us estimate the interface thickness. The lengths over which rapid decreases in Fig. 2 occur yield interface thicknesses $t_{Cu/V} = t_{Cu/Nb} = 0.6 \pm 0.1$ nm and $t_{Cu/W} = 0.9 \pm 0.1$ nm. The lack of any initial rapid decrease with CuPt is due to the absence of any interface between CuPt and Cu, and the smallness of any decrease with Ag is consistent with the independently measured⁷ very small value of $AR_{Cu/Ag} = 0.044 \pm 0.003$ fΩm².

We attribute the later slower decrease in $A\Delta R$ with t_N to the combination of increasing insert resistance [denominator of Eq. (1)] and spin-relaxation in N [numerator of Eq. (1)].

TABLE I. Independently measured resistivities, and derived parameters, for metal layers or multilayers.

Metal or Multilayer	ρ (nΩm)	l_{sf}^N (nm)	$AR_{Cu/N}$ (fΩm ²)	$\delta = t_{Cu/N}/l_{sf}^{Cu/N}$
CuPt(6 at. %)	160 ± 30	11 ± 3		
Ag	7 ± 2	>40		
V	105 ± 20	>40		
Nb	78 ± 15	25^{+5}_{-5}		
W	92 ± 10	4.8 ± 1		
Cu/Ag			0.044 ± 0.003	0
Cu/V			1.15 ± 0.15	0.07 ± 0.04
Cu/Nb			1.10 ± 0.15	0.19 ± 0.05
Cu/W			1.55 ± 0.1	0.96 ± 0.1

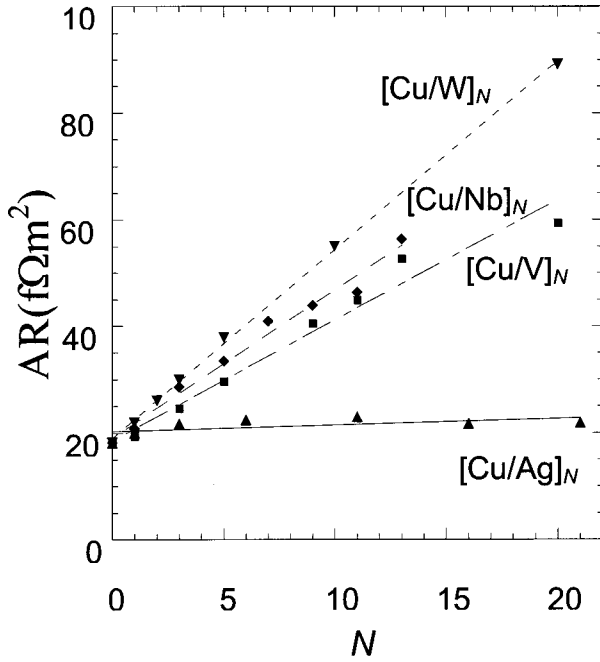


FIG. 7. $AR(AP)$ vs N for $[Cu/Ag]_N$, $[Cu/V]_N$, $[Cu/Nb]_N$, and $[Cu/W]_N$ multilayer inserts.

For Ag and V the predicted (solid) curves using independently measured parameters and assuming no spin-relaxation are so close to the data that we can only say that l_{sf}^{Ag} and l_{sf}^V are >40 nm, the maximum l_{sf}^N that we can distinguish from ∞ with the layer thicknesses measured. This expectedly long l_{sf}^{Ag} shows that our technique does not produce spurious spin-memory loss in single layers. For W, the predictions without spin-relaxation lie well above the data. The dashed curve through the W data in Fig. 6 is a fit with the value of $l_{sf}^W = 4.8$ nm given in Table I. The dashed curve through the Nb data in Fig. 6 is for $l_{sf}^{Nb} = 25$ nm. Both the W and Nb fits include also interfacial relaxation using the δ parameters in Table I. The fit to the Nb data is not unique. Those data can be fit with values of $20 < l_{sf}^{Nb} < \infty$ nm. A very long l_{sf}^{Nb} agrees best with Ref. 9. However, our fits to the $[Cu/Nb]_N$ data in Fig. 8 below, or to our previously published¹⁶ $[Cu/Nb]_N$ data, are then not so good. To “explain” the $[Cu/Nb]_N$ data we would have to invoke an additional interfacial contribution in Fig. 6 for intermediate Nb thicknesses, which would also have to explain the observed variation in falloff rate with different Nb thicknesses in Ref. 16. In contrast, the value $l_{sf}^{Nb} = 25$ nm also fits reasonably well the data of Fig. 8 (broken curve) and of Ref. 16.

We are now ready for our multilayer data. Figure 7 shows that $AR(AP)$ increases linearly with N . The slopes of these curves represent the added specific resistances per inserted bilayer. From these slopes, plus separate measurements of Cu and N films, we determined the values of $AR_{Cu/N}$ listed in column 4 of Table I. Armed with the materials parameters in the first three columns of Table I, obtained from the data in Figs. 6 and 7 and independently measured resistivities of separately sputtered thin films of each metal listed in column 2 of Table I, we can determine the parameters for our EBSVs with multilayer inserts and predict the decreases in ΔR with N in the limit of no spin-relaxation at the insert interfaces. For $[Cu/Ag]_N$ the prediction—solid curve in Fig.

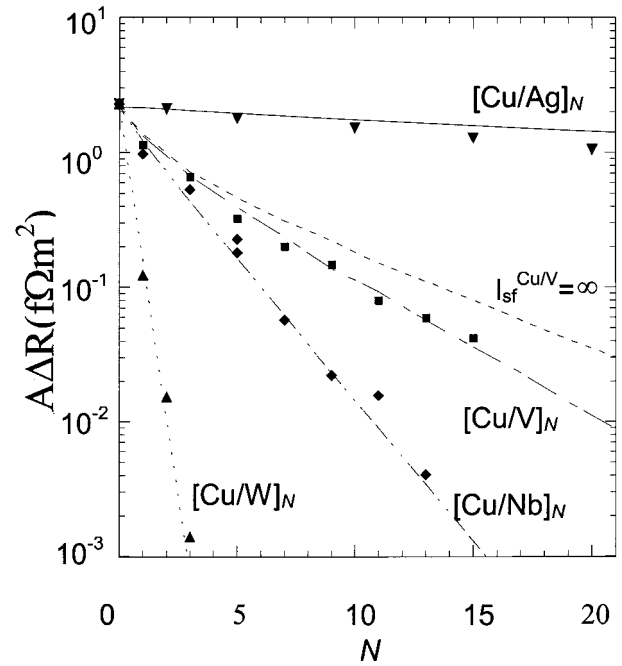


FIG. 8. $A\Delta R$ vs N for $[Cu/Ag]_N$, $[Cu/V]_N$, $[Cu/Nb]_N$, and $[Cu/W]_N$ multilayer inserts with fixed 3 nm thick layers of Ag, V, Nb, and W. The solid curve for Ag and the dotted curve for V are predictions for $\delta=0$ (i.e., $l_{sf}^{Cu/V} = \infty$). The dashed curves for V, Nb, and W are fits to the data using the values of δ given in Table I.

8—is so close to the data that we need little if any interfacial spin relaxation ($<0.5\%$ /interface). As Cu and Ag are chemically similar, and the Cu/Ag interface resistance is small,²⁷ this result is expected, and serves as an additional check on the validity of our technique. For the other three metals in Fig. 8, however, the data fall well below the predicted curves—e.g., the dotted curve for $[Cu/V]_N$. Best fits to the data with the analysis described in Sec. III above gives the values in Table I for $\delta = t_{Cu/N} / l_{sf}^{Cu/N}$. The values of δ for Cu/V, Cu/Nb, and Cu/W are surprisingly large for non-magnetic interfaces.

To try to explain the values of $AR_{Cu/N}$ and δ in Table I, we assume simple intermixing of the interfaces during sputtering to make a 50%/50% interfacial alloy, and we assume that this alloyed region is characterized by the independently measured bulk resistivity of the 50%/50% alloy. This model neglects effects of interfacial potential steps, an approximation seemingly justified by a recent calculation.²⁸

In this model, $AR_{Cu/N}$ should be given just by $\rho_{Cu/N} t_{Cu/N}$, where $\rho_{Cu/N}$ is the resistivity of the 50%/50% interfacial alloy, and $t_{Cu/N}$ is the interface thickness. From Fig. 6, as well as independent studies of interface thicknesses for our sputtered multilayers,²⁷ we estimate the thicknesses $t_{Cu/N}$ given above. The small $AR_{Cu/Ag}$ for our sputtered Cu/Ag multilayer has been satisfactorily explained elsewhere²⁷ simply by interfacial intermixing. No independent values of $AR_{Cu/N}$ for the other alloys exist. For these, we compare our new values of $AR_{Cu/N}$ with $\rho_{Cu/N} t_{Cu/N}$, taking for $\rho_{Cu/N}$, independently measured values for “bulk” Cu(50%)/V(50%), Cu(50%)/Nb(50%), and Cu(50%)/W(50%) alloys, or multilayers with short modulation wavelengths, all of which appear to be $\sim 150 \mu\Omega \text{ cm}$.²⁹ For V and Nb, $t_{Cu/N} = 0.6$ nm then gives

$AR_{\text{Cu/N}} = 0.9 \text{ f}\Omega\text{m}^2$, and for W, $t_{\text{Cu/W}} = 0.9 \text{ nm}$ gives $AR_{\text{Cu/W}} = 1.4 \text{ f}\Omega\text{m}^2$, all close to the values in Table I.

We next ask if our derived values of δ can be due simply to spin-orbit scattering within the same 50%/50% alloy of thickness 0.6 or 0.9 nm. We start with the equation for l_{sf} given in Ref. 11 in terms of λ_{el} , the elastic mean-free-path, and λ_{sf} , the spin-flip-length (we shall assume $\lambda_{\text{sf}} = \lambda_{\text{so}}$, the spin-orbit length):

$$l_{\text{sf}} = \sqrt{(\lambda_{\text{el}}\lambda_{\text{sf}}/6)}. \quad (5)$$

For a dilute alloy, λ_{el} can be written as $C/\rho_{\text{Cu/N}}$, where C is a constant associated with the ‘‘host metal’’ and $\rho_{\text{Cu/N}}$ is the alloy residual resistivity.³⁰ For our assumed 50%/50% alloys, C should involve both metals in a way that we do not know. As the simplest choice, we take the host metal to be Cu, giving $\lambda_{\text{el}} = 66 \text{ nm}/(\rho_{\text{Cu/N}})$.³⁰ The resulting uncertainty is probably a factor of 2. As noted just above, independent measurements for N=V, Nb, and W all give $\rho_{\text{Cu/N}} \sim 150 \mu\Omega \text{ cm}$.²⁹ We thus take $\lambda_{\text{el}} = 66 \text{ nm}/150 = 0.44 \text{ nm}$ for all three alloys. This small value partly explains the short values of l_{sf} .

The λ_{sf} due to spin-orbit coupling was recently shown to be very sensitive to details of Fermi surface structure.¹⁵ From simple arguments we can thus expect only order of magnitude results. Dimensional arguments suggest that the relevant cross-section should scale with the fourth power of the atomic charge Z for a given valence.²¹ From Eq. (5) and the constant value just above for λ_{el} , the values of δ for V:Nb:W should then scale as 1:3:10 (i.e., as Z^2), similar to the observed 1:3:14.

Using a calculated spin-orbit cross-section σ_{so} for V in Cu,³¹ and the relation $\lambda_{\text{so}} = 1/(cn\sigma_{\text{so}})$, where $c = 0.5$ is the V concentration and n is the number of atoms/unit volume in Cu, we estimate for V in Cu that $l_{\text{sf}} = 1.2 \text{ nm}$ and $\delta = 0.5$. This estimate of δ is even larger than we observe, but the right order of magnitude. Given that the estimate applies dilute-limit values for λ_{el} , σ_{so} , and n to a 50%/50% alloy, and the apparent importance of Fermi surface details,¹⁵ this level of agreement seems satisfactory.

V. SUMMARY AND CONCLUSIONS

To summarize, we have described in detail and tested a technique for measuring spin-relaxation in nonmagnetic metal layers and at nonmagnetic metal-nonmagnetic metal interfaces. For measurements within single layers, the technique has the advantages that the current is uniform across the sample and the parallel (P) and antiparallel (AP) magnetic states of the system are under complete control. It also has the unanticipated advantage of allowing monitoring of the growth of the interfaces between the insert layer of interest and the Cu used to magnetically separate the magnetic layers. For measurements at interfaces, it seems to be more straightforward to analyze than ESR and probably more widely applicable. Tests of the technique for single metals using CuPt and Ag gave satisfactory agreement with previous measurements or expectation. The measured spin-relaxation for FeMn is so strong that we describe it just by an interfacial spin-relaxation of roughly 90%/interface. Combining new experimental data with the measured values of l_{sf}^{N} for our sputtered layers with N=Ag, V, Nb, and W, we are able to estimate values for spin-relaxation at Cu/Ag, Cu/V, Cu/Nb, and Cu/W interfaces. The spin-relaxation at Cu/Ag interfaces is expectedly small. In contrast, spin relaxation at Cu/V, Cu/Nb, and Cu/W interfaces is surprisingly large. However, both the large sizes, and the relative magnitudes, are compatible with a crude model where the interface is approximated as a Cu(50%)N(50%) alloy in which spin-relaxation is due to spin-orbit coupling. If this analysis is correct, it is important, since it would then be unnecessary to invoke potential steps at the interfaces to understand either the interface specific resistance or the interfacial spin-relaxation, thereby simplifying analysis of spin-relaxation for devices involving diffusive transport of spins across interfaces.

ACKNOWLEDGMENTS

This work was supported in part by the MSU CFMR, MSU CSM, and by the US NSF under DMR Grants No. 94-23795 and 98-20135 and MRSEC Grants No. 94-00417 and 98-09688.

*Present address: Physics Dept., Indiana University, Bloomington IN.

†Present address: Physics Dept., Calvin College, Grand Rapids, MI.

¹See, e.g., P. M. Tedrow and R. Meservey, Phys. Rev. Lett. **26**, 192 (1971); I. A. Campbell and A. Fert, *Ferromagnetic Materials*, edited by E. P. Wohlfarth (North Holland, New York, 1982), Vol. 3, p. 748.

²M. N. Baibich *et al.*, Phys. Rev. Lett. **61**, 2472 (1988); G. Binash *et al.*, Phys. Rev. B **39**, 4828 (1989).

³J. M. Daughton, J. Magn. Magn. Mater. **192**, 334 (1999); G. A. Prinz, *ibid.* **200**, 57 (1999).

⁴T. Valet and A. Fert, Phys. Rev. B **48**, 7099 (1993).

⁵J. Ph. Ansermet, J. Phys.: Condens. Matter **10**, 6027 (1998).

⁶M. Johnson and R. H. Silsbee, Phys. Rev. **55**, 1790 (1985).

⁷S. Steenwyk *et al.*, J. Magn. Magn. Mater. **170**, L1 (1997); W. P. Pratt, Jr. *et al.*, IEEE Trans. Magn. **33**, 3505 (1997).

⁸P. M. Levy, *Solid State Physics Series*, edited by H. Ehrenreich and D. Turnbull (Academic Press, New York, 1994), Vol. 47, p. 367; M. A. M. Gijs and G. Bauer, Adv. Phys. **46**, 285 (1997); J.

Bass *et al.*, Comments Condens. Matter Phys. **18**, 223 (1998).

⁹M. Johnson, Appl. Phys. Lett. **65**, 1460 (1994), and references therein.

¹⁰Q. Yang *et al.*, Phys. Rev. Lett. **72**, 3274 (1994).

¹¹A. Fert, J.-L. Duvail, and T. Valet, Phys. Rev. B **52**, 6513 (1995).

¹²L. Piraux *et al.*, J. Magn. Magn. Mater. **156**, 317 (1996); A. C. Reilly *et al.*, *ibid.* **195**, L269 (1999); W. Park *et al.*, J. Appl. Phys. **85**, 4542 (1999).

¹³S. Y. Hsu *et al.*, Phys. Rev. B **54**, 9027 (1996).

¹⁴F. Taddei *et al.*, Phys. Rev. Lett. **82**, 4938 (1999).

¹⁵J. Fabian and S. Das Sharma, Phys. Rev. Lett. **81**, 5624 (1998).

¹⁶D. V. Baxter *et al.*, J. Appl. Phys. **85**, 4545 (1999).

¹⁷W. P. Pratt, Jr. *et al.*, Phys. Rev. Lett. **66**, 3060 (1991).

¹⁸B. Dieny *et al.*, J. Appl. Phys. **69**, 4774 (1991).

¹⁹R. Magno and J. H. Pifer, Phys. Rev. B **10**, 3727 (1974).

²⁰We used W instead of Ta because rapidly sputtered Ta adopts a complex structure with a very high resistivity that overwhelms any spin-relaxation in our structures.

²¹J. S. Griffith, *The Theory of Transition-Metal Ions* (Cambridge

- University Press, Cambridge, 1964); Y. Yafet, *Solid State Physics*, edited by F. Seitz and D. Turnbull (Academic, New York, 1963), Vol. 14, p. 1.
- ²²M. Hanson and K. Anderko, *Constitution of Binary Alloys*, 2nd ed., Metallurgy and *Metallurgical Engineering Series*, edited by R. P. Mehl (McGraw-Hill, New York, 1958).
- ²³S. F. Lee *et al.*, Phys. Rev. B **52**, 15 426 (1995); J. M. Slaughter *et al.*, Rev. Sci. Instrum. **60**, 127 (1989).
- ²⁴C. Tang and K. Lee, J. Appl. Phys. **53**, 2605 (1982).
- ²⁵S. F. Lee *et al.*, J. Magn. Magn. Mater. **118**, L1 (1993).
- ²⁶L. Vila *et al.*, J. Appl. Phys. **87**, 8610 (2000).
- ²⁷L. L. Henry *et al.*, Phys. Rev. B **54**, 12 336 (1996).
- ²⁸P. Zahn *et al.*, Phys. Rev. Lett. **80**, 4309 (1998).
- ²⁹K. H. Breckler *et al.*, Z. Phys. Chem., Neue Folge **157**, 401 (1988); T. R. Werner *et al.*, Phys. Rev. B **26**, 2224 (1982); J. Ivkov *et al.*, Solid State Commun. **88**, 633 (1993).
- ³⁰N. W. Ashcroft and N. D. Mermin, *Solid State Physics* (Saunders, Philadelphia, 1976); J. Bass, in *Metals: Electronic Transport Phenomena*, edited by K.-H. Hellwege and J. L. Olsen, Landolt-Börnstein, New Series, Group III, Vol. 15a (Springer-Verlag, Berlin, 1982), pp. 1–287.
- ³¹P. Monod and S. Schultz, J. Phys. (Paris) **43**, 1564 (1971).